o be submitted to
iclear Instr. and Meth.

COMITATO NAZIONALE PER L'ENERGIA NUCLEARE
Laboratori Nazionali di Frascati

LNF-74/45(P)
5 Agosto 1974

F. Balestra, R. Barbini, L. Busso, I. V. Falomkin, R. Garfagnini, C. Guaraldo, M. M. Kulyukin, G. Perno, G. Piragino, G. B. Pontecorvo, R. Scrimaglio and Yu. A. Shcherbakov:

SELF SHUNTED STREAMER CHAMBER. -

Servizio Documentazione
dei Laboratori Nazionali di Frascati del CNEN
Casella Postale 70 - Frascati (Roma)

Laboratori Nazionali di Frascati del CNEN
Servizio Documentazione

LNF-74/45(P)
5 Agosto 1974

F. Balestra(x), R. Barbini, L. Busso(x), I.V. Falomkin(o), R. Garfagnini(x), C. Guaraldo, M.M. Kulyukin(o), G. Perno(x), G. Piragino(x), G.B. Pontecorvo(o), R. Scrimaglio and Yu.A. Shcherbakov(o):

SELF SHUNTED STREAMER CHAMBER. -

ABSTRACT. -

The self shunted streamer chambers can be used as visualizers of particles' tracks and as detectors of events' vertex. We discuss the operating conditions of this type of chamber in the presence of a magnetic field and the features of the H.V. pulse generator connected to the chamber. The results upon the precision which can be obtained in the reconstruction of the tracks are discussed.

(x) - Istituto di Fisica dell'Università di Torino, and Istituto Nazionale di Fisica Nucleare, Sezione di Torino.

(o) - Joint Institute for Nuclear Research, Dubna (URSS).

1. - INTRODUCTION. -

In the last years the use of streamer chambers in nuclear and high energy physics has been increasing rapidly: by consequence, the technical development of such devices has gained a great enhancement[1, 2].

Basically, two types of streamer chambers can be distinguished: those in which the H. V. pulse is quenched in order to prevent from propagation of the discharge in the surroundings of the ionizing particles path[3], and those in which the H. V. pulse is quenched by the discharge in the chamber itself[4] (self shunted streamer chambers). The localization of trajectories turns out to be similar in both types of chambers. For the first type of chambers, however, the poor brightness of tracks requires the use of filling gas mixtures usually consisting in 70÷90% of Ne and 30÷10% of He, together with image intensifiers and special attentions for obtaining a short (10÷20ns) H. V. pulse (Blumlein system). In the chambers of the second type, the most suited impurities to be added to the filling gas (^{3}He; ^{4}He) must be found in order to achieve the best localization of tracks, which are very bright. Usually one has to deal with hydrocarbons in percentages of few parts per thousand[4].

The self shunted streamer chambers have also the advantage of operating, filled with high purity ($\gtrsim$ 99.9%) helium, even at high pressure[5, 6]. On the other hand a disadvantage arose during the experiment[7], in which a self shunted streamer chamber, filled with He at one atm, and placed in a magnetic field, was used for analysing $\pi^{\pm}$ beams. Namely, it turned out that, because of the magnetic field, the tracks loosed their vertical localization (Fig. 1), at least if the usual percentage[4] of contaminating hydrocarbons were used.

In this paper we describe the operating conditions of a self shunted streamer chamber used as a tracks' visualizer in a magnetic spectrometer[8]. In particular we discuss how good localization can be achieved by replacing hydrocarbons with suitable inorganic gases for contaminating the chamber's filling gas. Finally, the results we obtained in the spatial tracks' reconstruction are also reported.

2.- DESCRIPTION OF THE EQUIPMENT.-

The magnetic spectrometer consists in a streamer chamber, inside a magnetic field, which has been exposed to the $\pi^{\pm}$ beam of the LEALE Laboratory in Frascati. The trigger for the H.V. pulse generator is provided by a counters' telescope as shown in Fig. 2.

2.1.- The electromagnet.-

The electromagnet has been built in the Frascati National Laboratories of CNEN[9]. It generates a uniform (within $\pm$ 0.5%) magnetic field inside a cylindrical volume 10 cm high and 42 cm in dia.. The uniformity has been achieved by introducing two iron rings into the coils, as schematized in Fig. 3. In Fig. 4 the field maps at three quotes are given for B = 7200 Gauss: they don't change appreciably in the range 5000 to 9000 Gauss (maximum field). This electromagnet allows for measuring radii of curvature with very high precision, for well localized tracks 30 ÷ 40 cm long[10].

2.2.- The H.V. pulse generator.-

As it is well known, for the operation of streamer chambers electric pulses a few hundreds of kV high and with peculiar time features are needed[11]. The most commonly used H.V. generators for this purpose are those of the Arkadiev-Marx type which show the following qualities: low output impedance, low self inductance,

stability in their parameters. The specific application of such generators for pulsing streamer chambers requires the fulfillement of additional conditions such as:

a) the possibility to be triggered with a delay as small as possible between input and output and a negligible jitter in this delay;
b) the capability of operating at the frequency required by the experiment;
c) to produce a H. V. pulse with a very fast ($\sim$ 10 ns) rise time;
d) to be provided with a sufficient number of sections and an overall discharge capacity for delivering the required output voltage to the load.

Each section consists of a capacity C which is charged through a resistance R and is separated from the next one by a spark gap.

The capacities C of the sections are all charged to the same voltage by connecting in series (Fig. 5) the charging resistors R. By triggering a discharge in the first section, we can obtain, as we shall see later, an over-voltage between the electrodes of the second spark-gap. The discharge between this two electrodes will give rise in turn to an over-voltage on the third section, and so on. The resulting over-voltage between the electrode of the last section and ground will then be approximatively the product of charging voltage V_o times the number n of sections. The discharging time of the H. V. generator depends upon the formation time of the discharge between the electrodes: for this reason the spark-gaps are mounted facing one another so as to allow for the ultraviolet flash and the ionization produced in each spark-gap to speed up the discharge. Moreover the spark-gaps' electrodes have been shaped with the least curvature still able to prevent for the stationary corona effect. If C_p is the stray capacitance between the sections and C_t the stray

capacitance of each section referred to the ground, we can draw for the second section (and subsequent) the equivalent circuit shown in Fig. 5 : V_S is the overvoltage which arises between the electrodes of the spark-gaps. The value and time behaviour of the overvoltage in the second spark-gap (lower than the overvoltage in the subsequent spark-gaps) can be deduced by the equivalent circuit of Fig. 5:

$$(1) \qquad V_s - V_o \leq V_o \frac{C_t}{C_t + C_p} e^{-\frac{t}{R(C_t+C_p)}}$$

By taking in account the average statistical delay of the discharge, which depends upon the operating conditions of the spark-gaps we can deduce the minimum value of R for a real H. V. generator. If for instance the output capacitance of a generator is $C_u = 357$ pF (we can obtain this capacitance for a generator with 14 stages of C = 5000 pF each) the resulting R turns out to be 10 kΩ about, which places an upper limit of about 10 Hz to the operating frequency of the H. V. generator. Since the charging time of the generator is higher by some orders of magnitude than the discharging time, it seems logical to replace the resistors R by inductances, which, by the way, are easier to be built: in this case the upper limit to the operating frequency will be determined by the deionization time of the spark-gaps. Basically, the rise time of the H. V. pulse depends upon the self inductance of the generator itself, which in turn depends upon the position, type and dimensions of the components used. It must be noted that the capacitors employed are anti-inductive, so that a generator turns out to be composed by n successive sections each consisting of m capacitors with nominal capacity C_o mounted in parallel. The generator is connected to a load capacitance C_c. Getting rid of the internal resistances, of the generator's self inductance and of the shunt effect due to the leakage currents, the output voltage V is approximatively given by the following relation:

$$V = \frac{m C_o}{m C_o + n C_c} n V_o \qquad (2)$$

The maximum operating frequency f, is given by:

$$f = \frac{2 W}{C_o V_o^2 mn} , \qquad (3)$$

where W is the power delivered by the supply. From (2) and (3) we can deduce the capacity of each generator's section, $C = mC_o$, and the number of sections. In fixing V we must recall that the actual amplitude of the output pulse can be reduced by $15 \div 20\%$[11]. In Fig. 6 an outline of the generator we built for this experiment is given. The generator is composed by 14 sections, with a capacitor each (5000 pF; 20 kV; $Ba\,Ti\,O_2$), it has molybden electrodes, with adjustable distances, and can operate in a nitrogen atmosphere at a pressure of up to 4 Atm. The first section is fired by a four electrodes system (see Fig. 6), three of which are mounted at right angles to each other while the fourth electrode consists of a platinum-iridium wire pushing on a $Ba\,Ti\,O_2$ pellet to provide a ultraviolet flash. This u.v. flash, which is seen also by the first spark-gap of the generator, keeps fairly constant the delay between the input and the output pulses (300 ns), within a very small jitter. The triggering system is shown in Fig. 7: it transforms the pulse provided by the electronic logic of the experiment into the pulse required to start the generator, namely $V_o/2$.

In Fig. 8 a sketch of the equipment is given. The generator is mounted inside a cylindrical inox steel vessel resting on an insulating ring which in turn is placed upon the lower iron magnetic field correction ring. The vessel contains also the cylindrical insulating support of the high voltage electrode, upon which the streamer chamber is laid.

The high voltage electrode (an aluminum plate 1.5 cm thick and 54 cm in dia.) is connected to the generator; both the plate and the connection are immersed in a bath of highly insulating ($\sim$ 100 kV/mm) oil. The ground wire electrode, placed at the top of the streamer chamber, is connected to the cylindrical vessel. This electrode is formed by a brass ring, with an internal diameter of 50 cm; upon this frame Ni-Cr wires (ϕ = 0.1 mm) are tightened with a spacing of 1 cm, which permits to photograph the chamber's interior. The discharge through the chamber ends on the generator's external metallic vessel and the ground of the chamber H.V. generator system is separated from the magnet's ground, which acts as an electrostatic screen.

In the presence of particles through the chamber, the H.V. pulse turns out to be 40 ÷ 70 ns long, in agreement with the results of ref. (11).

2.3.- The streamer chamber.-

The streamer chamber shown in Fig. 8 is the last of a series of models we have tested. It has an internal diameter of 52 cm and an internal height of 12 cm. The diameter has been so choosen as to photograph only the chamber's portion where the magnetic field is constant, avoiding in the same time to photograph the vertical wall, and 2 ÷ 3 cm of track near the wall itself. The cylindrical wall is made of PVC (polivynilchloride) 0.5 cm thick; the thickness is reduced to 0.3 cm in the region traversed by the particles. The cylinder is closed on top an bottom by two glass plates 1 cm thick. The internal surface of the cylinder has been painted in black with a suitable pigment dissolved in araldite. A glass tap has been inserted in the cylindrical wall for filling and draining the chamber. Finally, a window (22 cm large and as high as the chamber is) has been cut away from the wall and covered with a thin (0.07 mm) PVC foil, glued to

the window's edges by araldite. The upper glass plate of the chamber has a diameter larger than the lower one (which is immersed in oil) in order to increase the external distance in air between the upper electrode and the inner surface of chamber's wall. Fiducial marks have been engraved on the surfaces of the glass plates and are illuminated together with the counter of pictures by grazing light just after the two cameras have advanced. The cameras are equipped with objectives MIR -1 (aperture f/2.8, focal length 37 mm), the optical axes are parallel to the electric and magnetic fields and are 160 mm apart. The centre of each objective has a distance of 789 mm from the chamber's bottom (ϕ = 520 mm) whose image in the picture results to be 24 mm in dia.. Between the two objectives a mirror has been mounted at 45 deg with respect to the chamber's axis in order to remotely monitor the chamber's operation via a television system.

These chambers require to be vacuum pumped for about 12 hours: when a static vacuum better than 10^{-2} torr has been reached, they are filled and drained with pure helium before the final filling.

2.4.- Streamer chamber filling technique.-

In a streamer chamber the discharge originates along the ionizing particle's path and propagates symmetrically towards the electrodes[12]. The possibility of reconstructing from stereo pictures the points of the particles trajectory (localization) is poor along the direction of the electric field while is good at right angle. This feature occurs both in the chambers pulsed by a short H. V. pulse[13,14] and in the self shunted chambers; in the latter case, however, the tracks are much more bright. The addition of hydrocarbons vapours improves the localization of tracks[4], allows for operation at pressure higher than the atmospheric one[5,6] and reduces the brightness of the two brush discharges which propagate symmetrically towards

the electrodes. This happens because the impurities have energy levels much lower than those of helium and high photoionization cross sections and are therefore able to reduce the mean energy of the electrons and, as a consequence, the number of excited helium atoms in the brushes. It follows a reduction in the brightness of the diverging brushes, while the brightness remains unchanged in the region where the electron density, and the number of excited helium atoms, is higher, i. e. in the region we define to be the "track". The best results up to now have been obtained by contaminating helium with vapours of α-pinene (refined oil of turpentine) in small amounts ($\leq 0.05\%$), and employing electric fields higher than 10 kV/cm at atmospheric pressure.

However it must be noted that hydrocarbons tend to decompose and loose their localizing effects after a few ten thousand discharges. Furthermore, vertical localization becomes to be lacking in streamer chambers whenever they operate in the presence of magnetic fields higher than 1 kG. This trouble is obviously absent in chambers where the H. V. pulse is short ($10 \div 15$ ns). During the operation of our chambers filled with helium and α-pinene we noticed that the applied magnetic field (parallel to the electric field) contracts the dimensions of the brush discharges and increases the spatial density of the charges. For a magnetic field of 1 kG, the electron density in the brush from the side of the positive electrode is enough for exciting the helium atoms, thus creating a bright oblong region above the point of the track, which appears as succession of exclamation points (!!!!!!). Fig. 9 shows an example of this type of tracks. Moreover, this phenomenon clearly indicates that the discharge is not propagating toward the two electrodes in a symmetric way. If the magnetic field is increased ($2 \div 3$ kG) a bright zone is created also toward the negative electrode. For fields higher than $4 \div 5$ kG

the discharge reaches both electrodes as seen in Fig. 2. Fig. 10 gives a sketch of the above arguments. For a fixed magnetic field value, the phenomenon can be diminished by reducing the α-pinene amount. Therefore, in order to avoid the disadvantage of vertical discharges (cases b, c, d of Fig. 10) which should prevent from using this type of streamer chambers in the presence of a magnetic field, we reduced the α-pinene contamination up to a limit which is below the sensitivity of filling equipment. As a consequence, we obtained unreproduciable contaminations, a lower photographic contrast of the tracks and a higher number of bright discharges along the vertical wall of the chamber. The picture in Fig. 9 has been taken with an applied magnetic field of 5 kG, with an α-pinene contamination which, by mistake, was slightly exceeding.

In order to overcome the difficulties related to the α-pinene contamination, we tried to reproduce the localizing effect by using a mixture of inorganic gases, which moreover, don't vary their characteristics when submitted to repeated electrical discharges.

Satisfactory results, from the point of view both of operation stability in a magnetic field and of track localization, have been obtained by contaminating helium with small amounts of Xe and N_2. Starting from a vacuum of 10^{-2} torr about, the chambers are filled with Xe up to 10^{-1} torr about, with N_2 up to 4×10^{-1} torr, at which point the filling is completed with He up to the atmospheric pressure. These values for pressures, recorded by the same instrument, represent the filling we consider the most suited for helium filled chambers at atmospheric pressure and in the presence of a magnetic field. By employing films with $27 \div 29$ Din Ilford HP4 sensitivity it is possible to photograph tracks of particles at minimum of ionization with an aperture f/5.6. There are no problems for recording in the same time α particles and $\pi^{\pm}$ mesons: Fig. 11 shows a (π^+, He^4)

large angle scattering event occurred during the experiment[8](x).

No bright brushes are now observed along the tracks. This means that the mean energy of electrons in the brushes is in this case higher than in the presence of α-pinene contamination, and the trapping effect of the magnetic field is therefore reduced. On the other hand, the energy of electrons is not yet enough for exciting the lowest emission levels of He in the visible spectrum.

The most relevant emission of He in the visible spectrum occurs at a wavelength of 5875.62 Å for an excitation energy of 23.07 eV (ref. 15). This corresponds to the emission of photons with an energy of about 2.1 eV and to a residual excitation energy of helium of about 21 eV (Helium does not emit for excitation energies lower than 20.95 eV). The residual excitation energy can be absorbed by impurities. Impurities must therefore be choosen which have the largest number of states excitable by an energy lower than 21 eV and corresponding to the emission of light not detectable by the usual photographic films. The organic molecules, for instance, emit intensively in the invisible spectrum. The electric field intensity must be the lowest which is consistent with a stable operation of the streamer chamber. In this way the energy of electrons in the brush discharges is high enough for exciting the lowest levels of impurities and only in the region where the spatial charge density is greatest both the highest levels of impurities, and the 23.07 eV level of He, can be excited. However, only very small percent contaminations must be employed, in order to keep negligible their emission in the visible spectrum, expecially from the brush regions. For instance, with

---

(x) - Furthermore, this problem does not exist either in high pressure chambers, as shown (see Fig. 12) by the (π^-, He^4) elastic scattering event taken in the experiment[7].

a N_2 contamination lower than 0.02% we obtain well localized tracks while the brush regions are bluish[16]; by increasing the amount of N_2, the localization is poorer because the visible emission of Nitrogen is no longer negligible.

The atomic excitation energies are well known[15], together with their relative intensities and is therefore possible to deduce the spectra shown in Fig. 13. The data referring to He, N, Ne, Ar, Kr and Xe are normalized among themselves in the range 5500 Å $\leq \lambda \leq$ $\leq$ 6000 Å. The full line hystogram represents the relative intensities as a function of wavelength (500 Å bins). The intervals $\lambda \leq$ 4000 Å and $\lambda \geq$ 7500 Å contain the total U.V. and I.R. emission respectively. By defining as "localizing power" for helium filled chambers the ratio between the emission intensity in the range 5500 Å $\leq \lambda \leq$ 6000 Å and the total intensity, we obtain for the various elements the results listed in Table I for different upper limits of the excitation energies. (We did not take in account the molecular spectrum of N_2, which emits mainly in the U.V. for excitation energies lower than 18 eV about).

It must however be noticed that the experimental conditions in which the emission spectra of ref. (15) have been obtained are different from those in which a streamer chamber normally operates.

From the values of Table I column 3, for excitation energies lower than 18 eV, it appears that the most relevant contributions to the localization of tracks are provided by N_2 and Xe.

This explanation can be extended also to the self-shunted streamer chambers filled with Ne, because this element has not energy levels lower than 18 eV[15]. Taking into account the interval 4500 Å $\leq \lambda \leq$ 6500 Å, also in the case of the neon filled chambers (see Table I) the best localization should be possible by contaminating with N_2.

TABLE I

Ratio between the emission intensity in the indicated vawe range and the total emission, for different upper limits of the excitation energies.

	Helium filled streamer chamber			Neon filled streamer chamber	
$\Delta\lambda$	(5500÷6000) Å total	(5500÷6000) Å ($\leq$21 eV)	(5500÷6000) Å ($\leq$18 eV)	(4500÷6500) Å total	(4500÷6500) Å ($\leq$18 eV)
He	0.087	---	---	0.113	---
N	0.036	0.038	0.013	0.152	0.042
Ne	0.096	0.146	---	0.472	---
Ar	0.055	0.066	0.077	0.216	0.236
Kr	0.058	0.062	0.068	0.219	0.203
Xe	0.055	0.055	0.058	0.359	0.378

Pion tracks, obtained in our selff-shunted streamer chamber filled with Ne contaminated with N_2, are shown in Fig. 14. The electric field was about 10 kV cm^{-1} and the objective aperture f/8; all the other experimental conditions were the same as in the case of He filled chamber. This result agrees with our phenomenological explanation of the track localization we obtained by adding a little amount of suitable impurities to the filling gases (helium or neon) of self shunted chambers.

3.- PRECISION IN THE TRACK RECONSTRUCTION.-

The photographic images of the tracks, obtained by two stereo-cameras, in the present experiment, have been measured with a semi-automatic plane digitizer and, in this case, it is possible to deduce with good precision the radius of curvature of the track. The precision depends [8] on the accuracy in the measurement of the tracks' points in each reprojection on the plane, on the track length and on value of the radius. In Fig. 15 the distribution of the distances of the points measured in a plane view from the best fit circle is shown; the result is in very good agreement with that of ref. (16) for straight line tracks. Measuring several times the pion track of Fig. 14 (L_π = = 28 cm) and the α-track of Fig. 11 (L_α = 13 long) we obtained the values of curvature radius shown in Fig. 16. The number of non corresponding points measured in each view is 15.

Better results in the recoil particle energy measurement can be obtained in the high pressure streamer chamber. It is possible, in this case, to deduce with good precision the range and angles of the tracks. For example, the method we used in the experiments [7] consists in measuring 5 points for each track in each view. When, for example, the α-recoil stops in the chamber (see Fig. 12 and 17)

the first point A and the fifth pont A' are selected at the ends of the track, as those having about the same darkness, since the α -tracks are very bright and their length in the photographic images depend also on the quality of the film development. After subtracting, in each view twice the segment A'V to the total length AA' the spatial reconstruction of the recoil results in good agreement with the kinematic previsions. For the event of Fig. 12 our reconstruction gives the results shown in Fig. 18. The incident pion energy value, deduced by these data, is $E_\pi = (181 \pm 4)$ MeV and in that exposition the central pion beam energy was (180 ± 9) MeV.

4. - CONCLUSIONS. -

The self-shunted streamer chambers are, as shown, good track detectors and also good vertex detectors, when their filling gas (^{4}He, ^{3}He, Ne) is used as target. The relatively low electric field necessary ($\simeq 10$ kV cm^{-1}) permits the construction of big volume chambers, but this type of chamber cannot work with a central H. V. electrode, as in the case of the short pulsed chambers[3]. The brightness of the tracks permit to use commercial film and a small objective aperture. The precision in the radius of curvature measurement is comparable to that obtainable with other visual detectors, but absolute measurements of track ionization are very difficult (see ref. (1) pag. 238). The range measurement, as known, is the best method for deducing the particles energy and in streamer chambers also it gives good results.

ACKNOWLEDGEMENTS. -

The authors would like to thank the Accademia Nazionale dei Lincei and the Professors C. Villi and V. P. Dzhelepov for their continuous encouragement and support. They are grateful to Mr. A. Benedetto and Mr. L. Valsana for the appreciated work on the streamer chambers. Finally they wish to thank the LNF-LEALE staff for the essential assistance throughout the experiment.

REFERENCES. -

(1) - Proc. of Streamer Chamber Technology Conf., ANL-8055 (1972).
(2) - Proc. of Instrumentation for High Energy Physics Conf., Frascati (1973).
(3) - G. E. Chikovani et al., Sov. Phys. -JETP 46, 1228 (1964); B. A. Dolgoshein et al., Sov. Phys. -JETP 46, 1953 (1964); F. Bulos et al., SLAC Rep. N. 74 (1967); A. Abashian et al., Nuclear Instr. and Meth. 115, 445 (1974).
(4) - I. V. Falomkin et al., Nuclear Instr. and Meth. 53, 266 (1967).
(5) - I. V. Falomkin et al., Nuovo Cimento 34, 1394 (1964).
(6) - I. V. Falomkin et al., ANL-8055 (1972), p. 121; Nuovo Cimento 5, 757 (1972).
(7) - I. V. Falomkin et al., Nuovo Cimento 3, 461 (1972); Preprint JINR, P1-7742, Dubna (1974); Nuovo Cimento, in press.
(8) - F. Balestra et al., Nuclear Instr. and Meth. 119, 347 (1974).
(9) - R. Garfagnini et al., Frascati report LNF-63/4 (1963).
(10) - L. Busso et al., Nuclear Instr. and Meth. 102, 1 (1972).
(11) - M. M. Kulyukin et al., Preprint JINR, P13-6533, Dubna (1972).
(12) - E. D. Lozansky and O. B. Firsov, Proc. of Intern. Conf. on Filmless Chambers, Dubna (1969), p. 89; O. B. Firsov, Sov. Phys-JETP 29, 367 (1969); E. D. Lozansky and G. B. Pontecorvo, Preprint JINR, P4-7529, Dubna (1973).
(13) - F. Rohrbach, ANL-8055 (1972), p. 81.
(14) - R. W. Morrison, ANL-8055 (1972), p. 167.
(15) - A. N. Saidel et al., Tablizi spektralnikh linii, (Nauka, Moscow, 1969).
(16) - L. Busso et al., Atti Accad. Sci. Torino 104, 423 (1970).

FIGURE CAPTIONS. -

FIG. 1 - Pion tracks in a self-shunted streamer chamber, filled with helium contaminated by α-pinene, in magnetic field (11 kG).

FIG. 2 - Layout of the experimental apparatus. $C_{1,6}$ = scintillation counters; 1) - (4x10) cm^2 collimator; 2) - analyzing magnet; 3) - streamer chamber; 4) - ^{12}C target (3x50x100) mm^3. The trigger for the H.V. pulse generator is given by the logic: $C_1C_2C_3\bar{C}_4C_5C_6$, in case of ref. (8), and $C_1C_2C_3C_4$ for this work.

FIG. 3 - Layout of the electromagnet. The zone of the magnetic field uniformity and his radial behaviour, obtained by introducing in the coils 1) two iron rings 2), are shown.

FIG. 4 - Magnetic field maps at different quotes. The full line represents the radial behaviour of the magnetic field after the correction.

FIG. 5 - Schematics of the H.V. pulse generator and equivalent circuit of the second section, V_o = charging voltage; V_s = overvoltage; C = capacity of each section; R = charging resistor; C_p = capacity between two sections; C_t = capacity of each section referred to the ground.

FIG. 6 - Outline of the H.V. pulse generator.

FIG. 7 - Outline of the triggering system. The pulse given by the electronic logic of the experiment is transformed into the pulse required to start the generator, namely $V_o/2$.

FIG. 8 - Layout of the streamer chamber placed in the electromagnet. 1) - stereo cameras; 2) - light sources for fiducial marks; 3) - connection strap between the upper wire electrode and the vessel containing the insulating oil for the H.V. electrode; 4) - streamer chamber; 5) - insulating oil; 6) - Arkadiev-Marx generator's container; 7) - connectors for charging power supply and trigger; 8) - tap for filling with N_2 up to 4 atm.

FIG. 9 - Pion tracks in a self-shunted streamer chamber, filled with helium contaminated by α-pinene (in percentage lower than in the case of Fig. 1), in magnetic field (5 kG). The real distance between the fiducial marks is 19.5 cm.

FIG. 10 - Front view of a track, in a self shunted streamer chamber, filled with helium at 1 atm and a little contamination of α-pinene ($\simeq$ 0.05 %), for different values of the magnetic field. a) - $<$1 kG; b) - $\simeq$1 kG; c) - 2-3 kG; d) - $\geq$4 kG.

FIG. 11 - (π^+, ^{4}He) elastic scattering event in a streamer chamber filled with helium at 1 atm and working in magnetic field. The real distance between the fiducial marks is 19.5 cm.

FIG. 12 - (π^-, ^{4}He) elastic scattering event in a streamer chamber filled with helium at 1 atm. The α-recoil is 79.6 mm long (see Figs. 17 and 18).

FIG. 13 - Atomic emission spectra of He, N, Ne, Ar, Kr, Xe. The data of ref. (15) are normalized in the interval 3500 Å $\leq \lambda \leq$ 6000 Å. The intervals $\lambda \leq$ 4000 Å and $\lambda \geq$ 7500 Å contain the total U.V. and I.R. emission respectively. The dashed line hystograms represent the emission spectra of the states excited by energies lower than 18 eV.

FIG. 14 - Pion tracks in a self-shunted streamer chamber, filled at 1 atm with neon contaminated by nitrogen. The maximum real distance between the fiducial marks is 19.5 cm.

FIG. 15 - Distribution of the distances of the measured points, in the plane views, from the best fit circle.

FIG. 16 - a) Radius of curvature of a pion track (28 cm long) measured several times (see Fig. 14); b) Radius of curvature of an α-recoil track (13 cm long) measured several times (see Fig. 11).

FIG. 17 - Schematics of the event of Fig. 12, as derived by each photographic view. The points AA' have been choosen, having about the same darkness, by the scanner. The segment R_α represents, for each view the projection of the α-recoil, independently from the quality of the film developments.

FIG. 18 - Distribution of the parameters (see Fig. 17) of the event of Fig. 12, measured several times. All the data have been reconstructed in the space. θ_π = angle of the elastic scattered pion; θ_α = angle of the α-recoil; R_α = range of the α-recoil. From these data the energy of the incident pion results $E_\pi = (181 \pm 4)$ MeV.

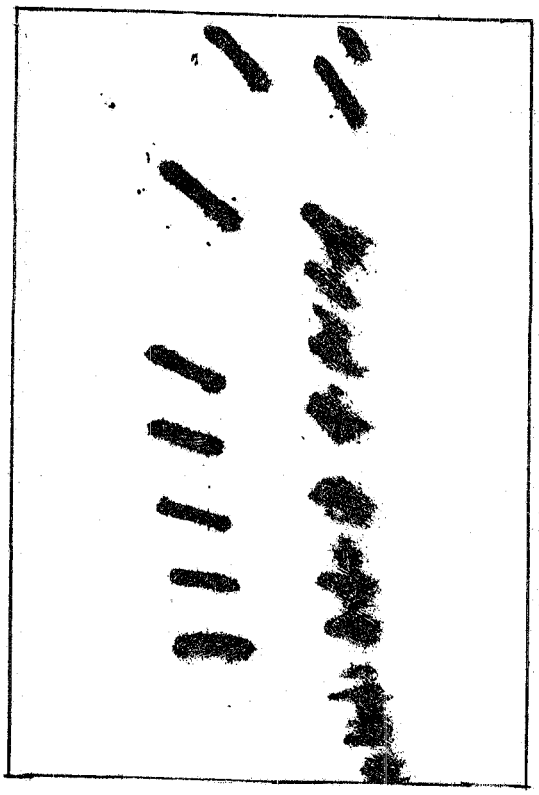

FIG. 1

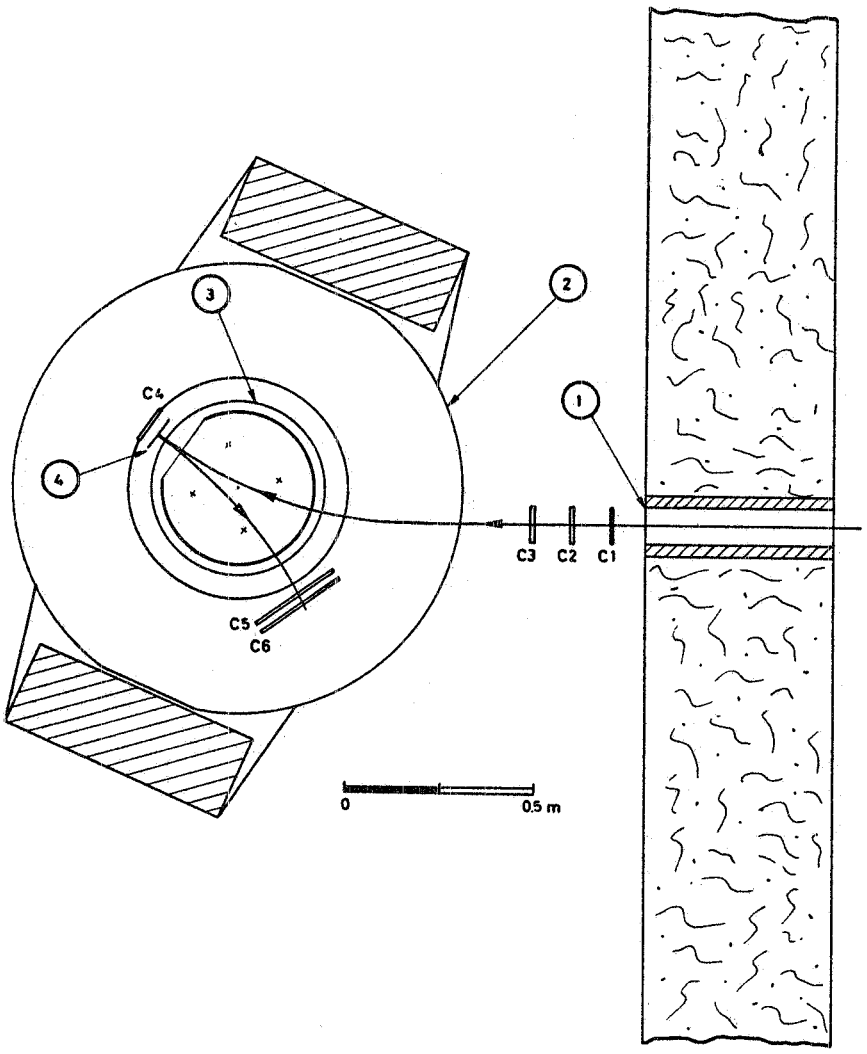

FIG. 2

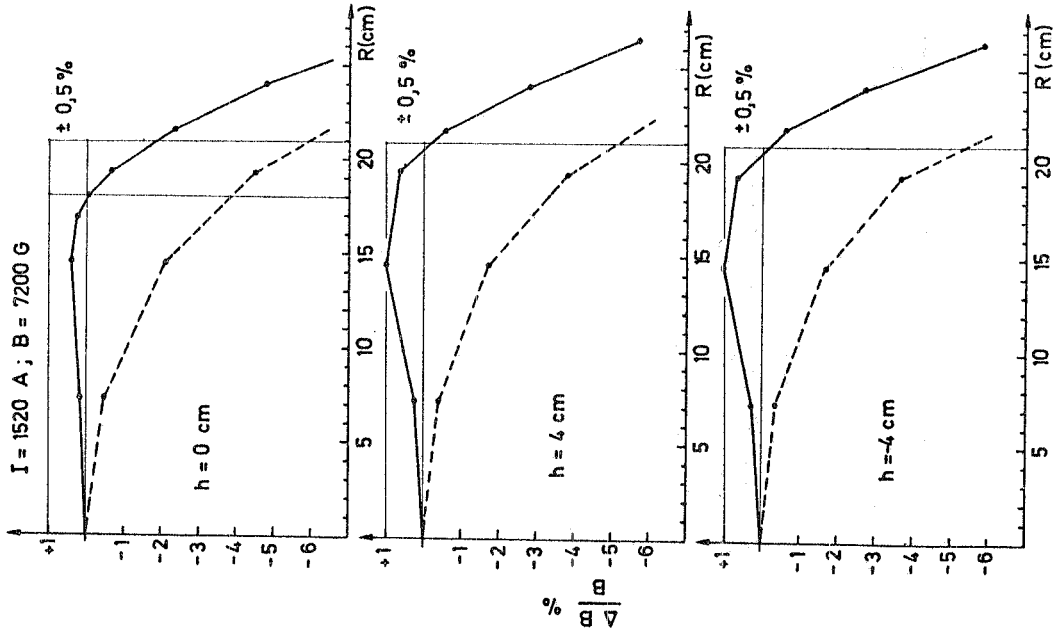
I = 1520 A ; B = 7200 G
± 0,5 %
h = 0 cm
h = 4 cm
h = -4 cm
R(cm)
Δ B/B %

FIG. 4

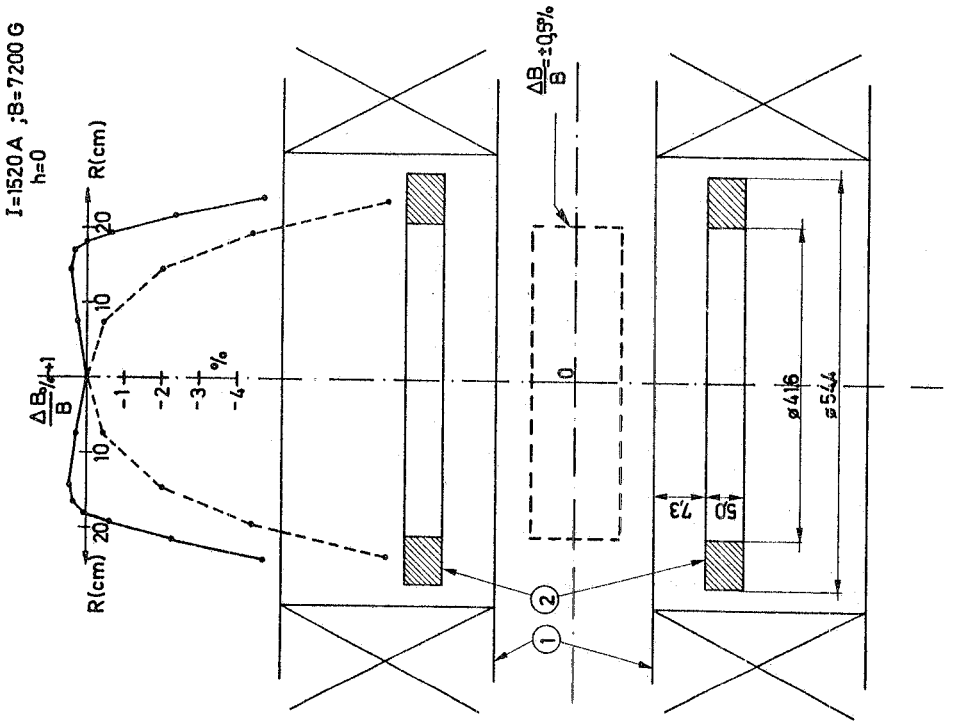
I=1520 A ;B=7200 G
h=0
R(cm)
ΔB/B
ΔB/B=±0,5%
ø416
ø544
73
50
1
2

FIG. 3

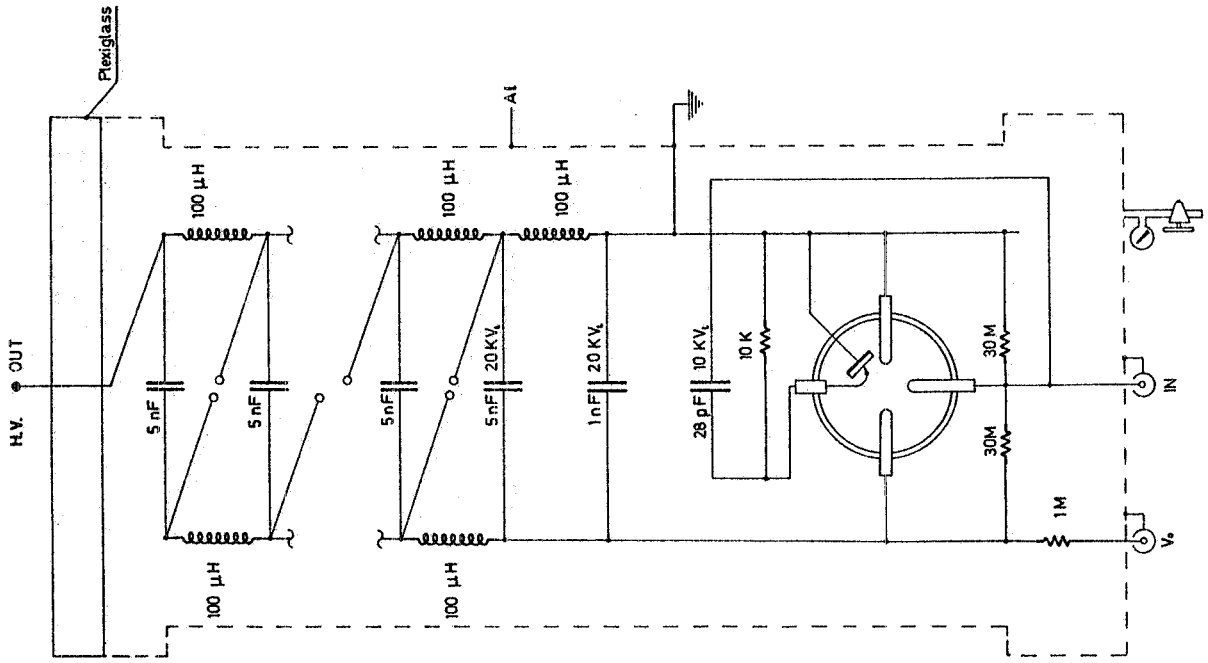
Plexiglass
Al
H.V.
OUT
100 μH
5 nF
5 nF
5nF
5nF
20 KVt
20 KVt
1nF
10 KVt
28 pF
10 K
30 M
30M
1 M
IN
Vo

FIG. 6

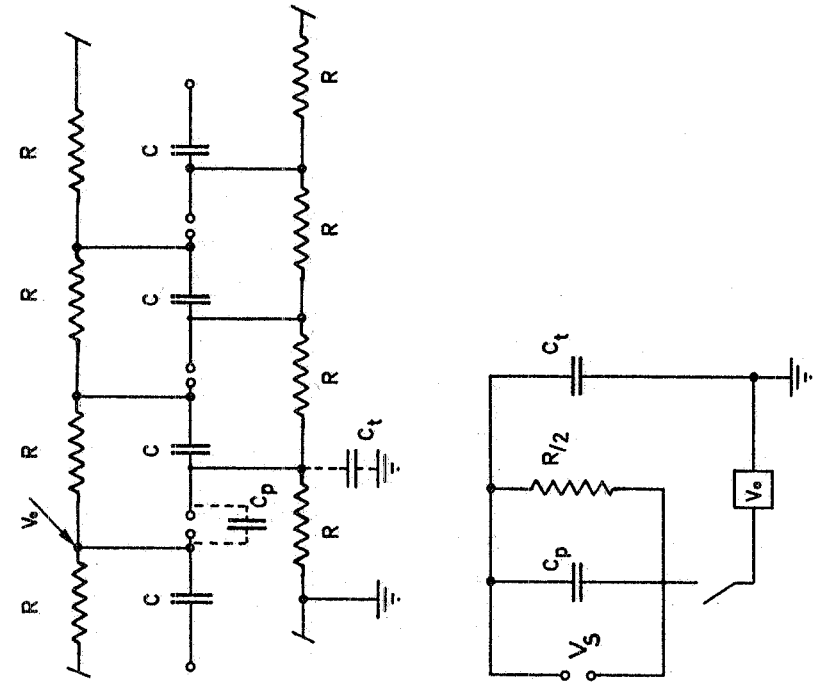
R
C
Ct
Cp
Vo
R/2
Vs

FIG. 5

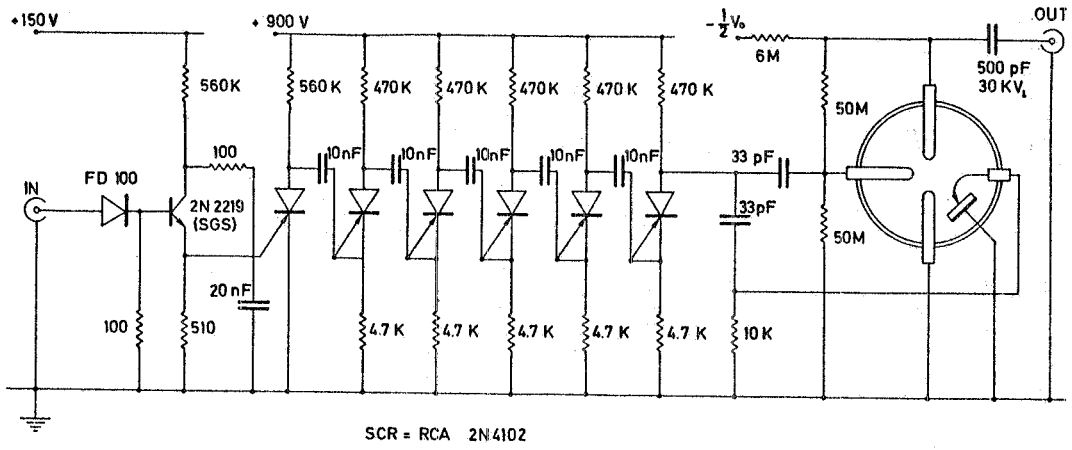
+150 V
+ 900 V
$-\frac{1}{2}V_o$
6M
OUT
500 pF
30 KV
560K
560 K
470 K
470 K
470 K
470 K
470 K
50M
100
10nF
10nF
10nF
10nF
10nF
33 pF
IN
FD 100
2N 2219
(SGS)
33pF
50M
20 nF
100
510
4.7 K
4.7 K
4.7 K
4.7 K
4.7 K
10 K
SCR = RCA 2N4102

FIG. 7

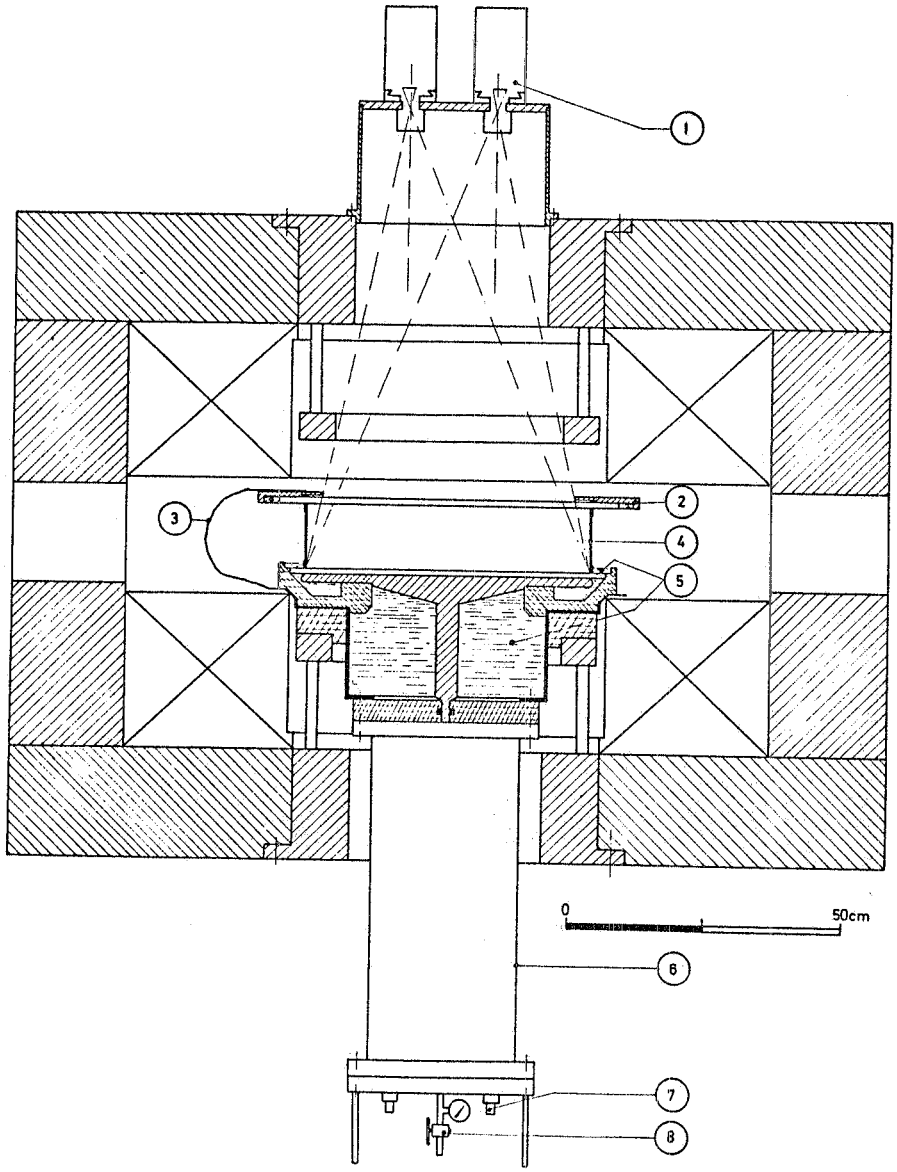
1
2
3
4
5
0
50cm
6
7
8

FIG. 8

FIG. 9

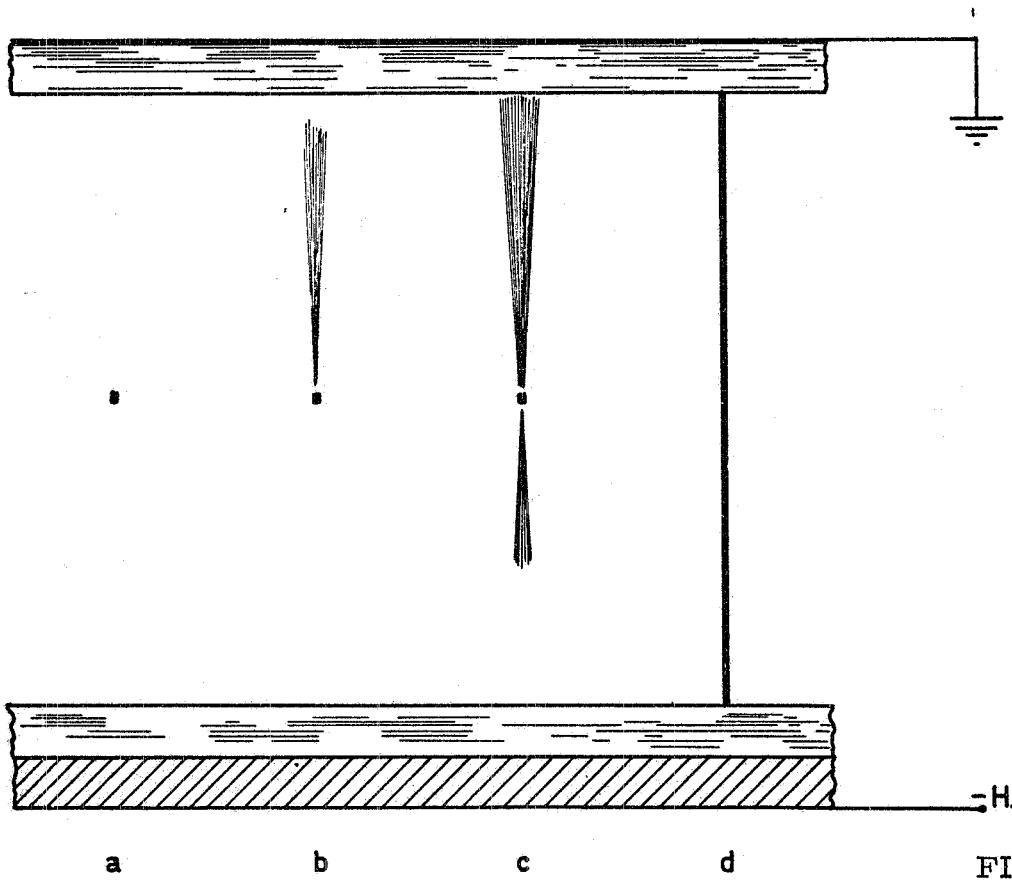

FIG. 10

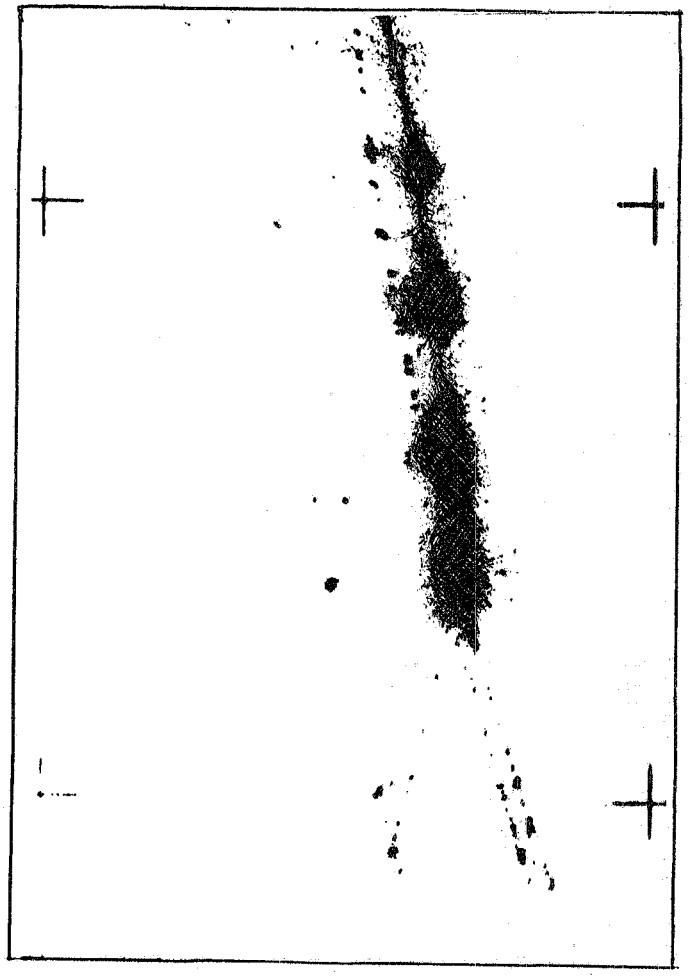

FIG. 11

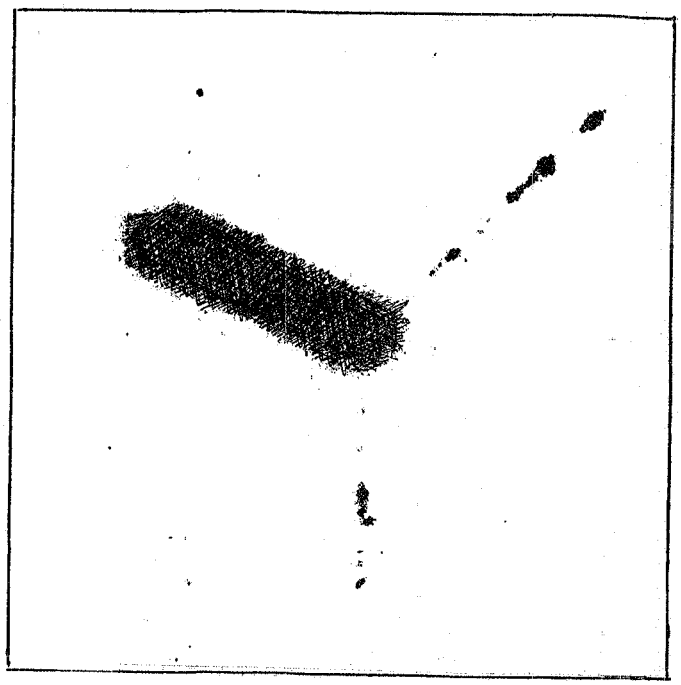

FIG. 12

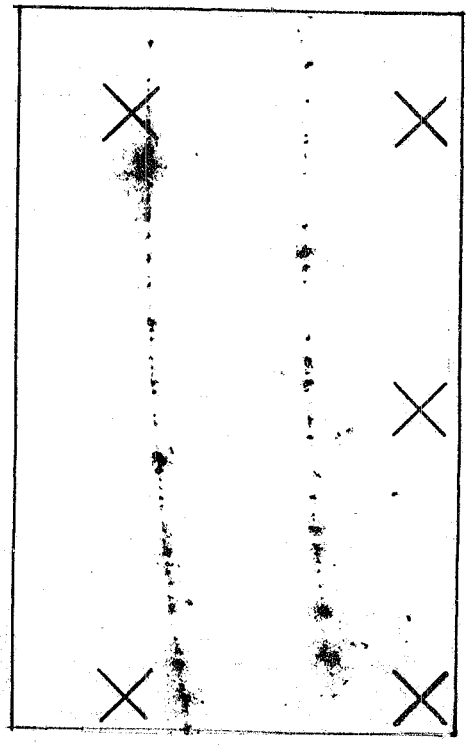

FIG. 14

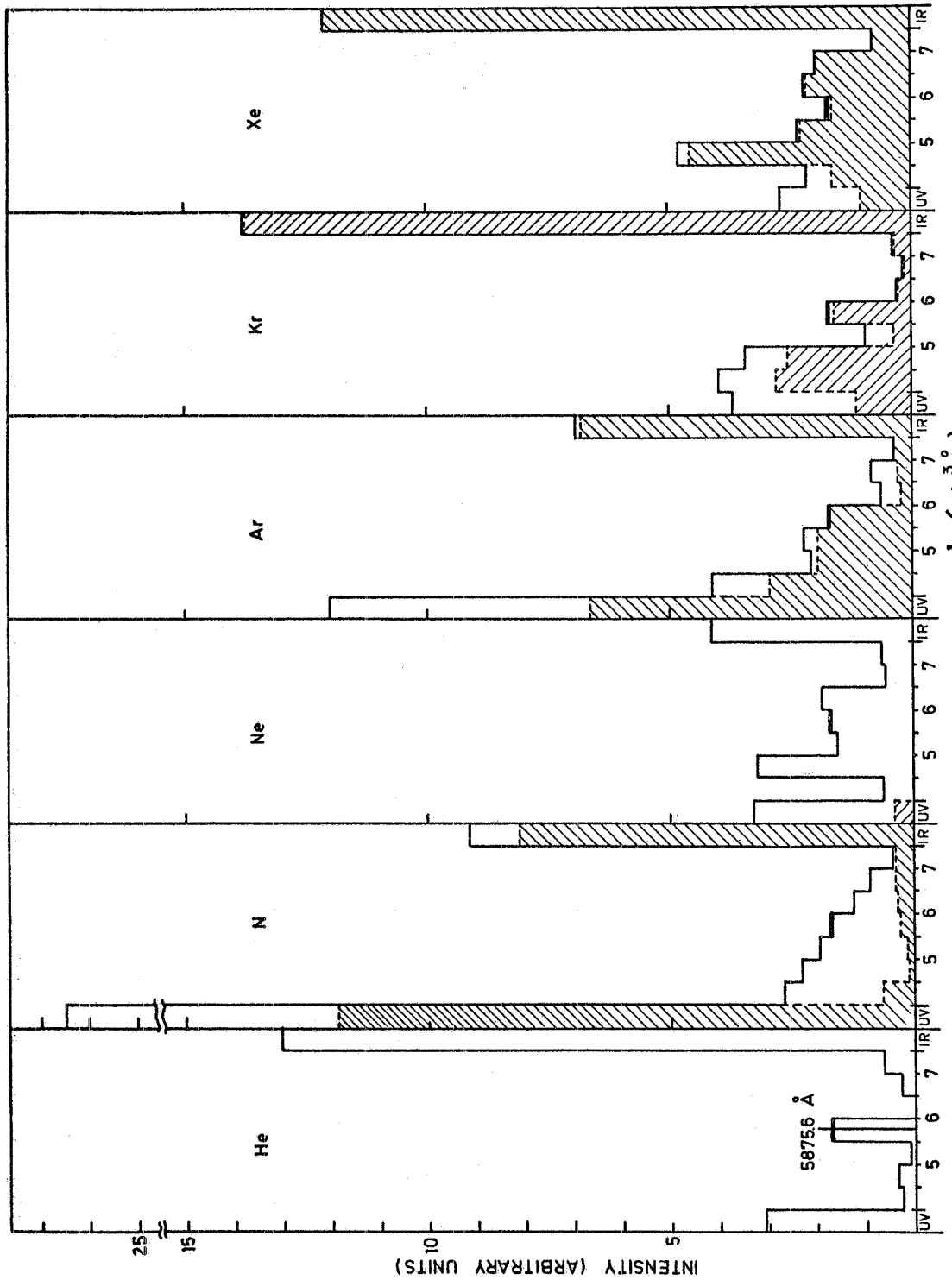
INTENSITY (ARBITRARY UNITS)
25
15
10
5
He
N
Ne
Ar
Kr
Xe
5875.6 Å
UV
IR
5
6
7
λ (x 10³ Å)

FIG. 13

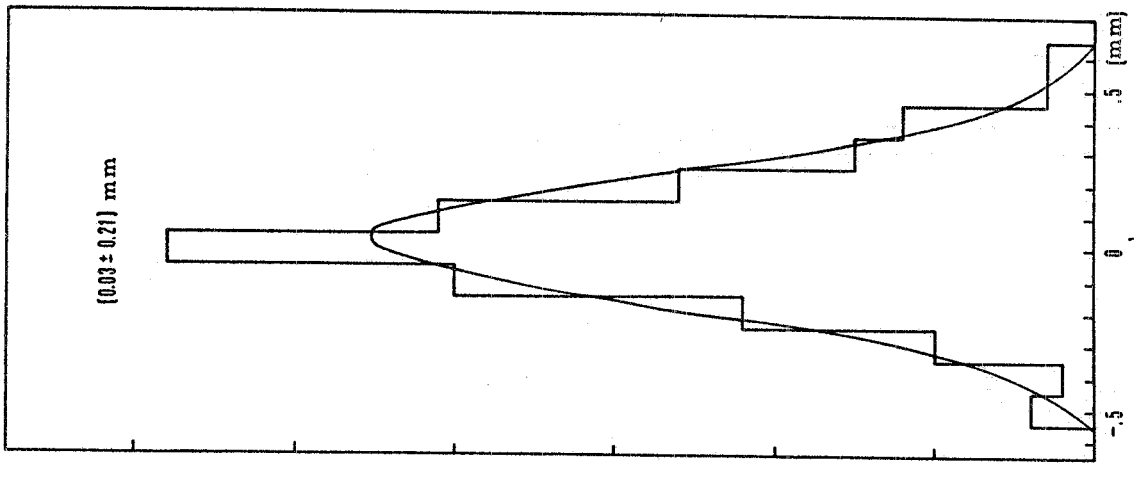
(0.03 ± 0.21) mm
-.5
0
.5 (mm)

FIG. 15

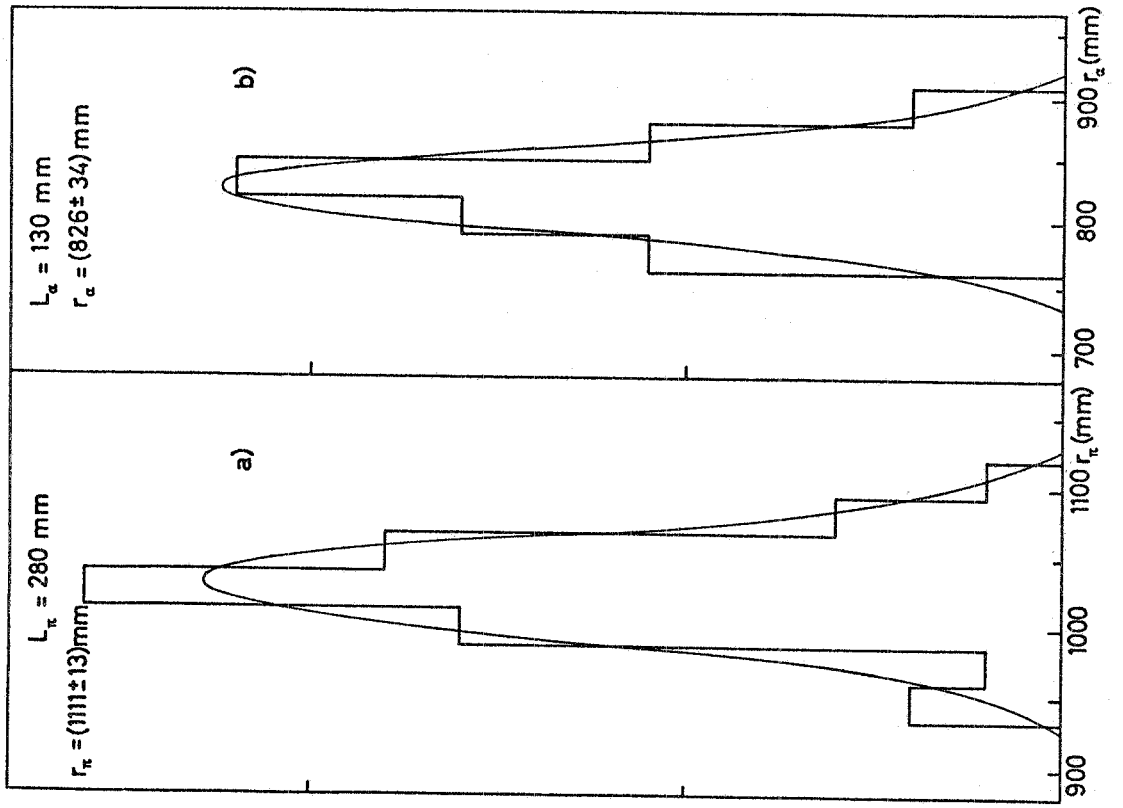
L_π = 280 mm
r_π = (1111 ± 13) mm
a)
L_α = 130 mm
r_α = (826 ± 34) mm
b)
900
1000
1100 r_π (mm)
700
800
900 r_α (mm)

FIG. 16

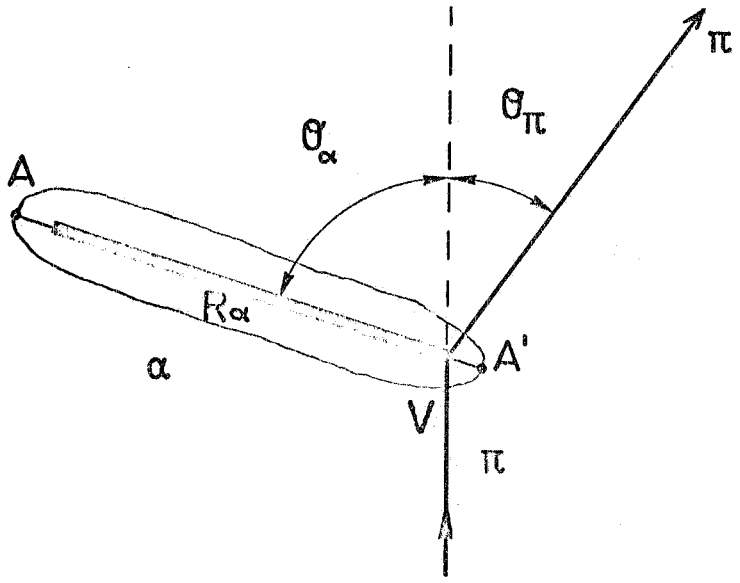
π
θπ
θα
A
Rα
α
A'
V
π

FIG. 17

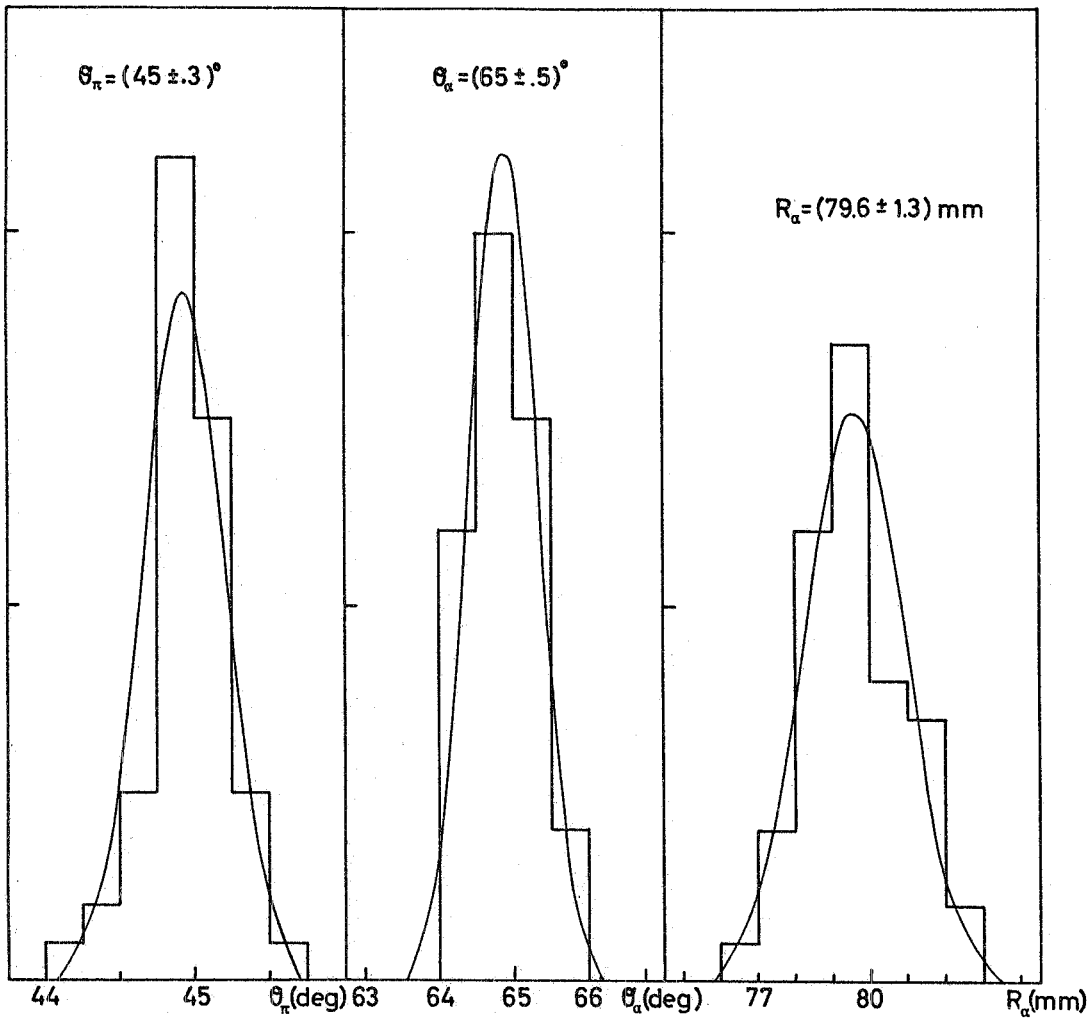
θπ = (45 ± .3)°
θα = (65 ± .5)°
Rα = (79.6 ± 1.3) mm
44
45
θπ(deg)
63
64
65
66
θα(deg)
77
80
Rα(mm)

FIG. 18